

Variational Quantum Computation of Molecular Linear Response Properties on a Superconducting Quantum Processor

Kaixuan Huang^{2,3,#}, Xiaoxia Cai^{1,#}, Hao Li^{3,7,#}, Zi-Yong Ge⁵, Ruijuan Hou¹,
Hekang Li³, Tong Liu^{3,4}, Yunhao Shi^{3,4}, Chitong Chen^{3,4}, Dongning Zheng^{3,4,6},
Kai Xu^{3,4,6,*}, Zhi-Bo Liu^{2,*}, Zhendong Li^{1,*}, Heng Fan^{3,4,6,*}, and Wei-Hai Fang¹

¹*Key Laboratory of Theoretical and Computational Photochemistry, Ministry of Education,
College of Chemistry, Beijing Normal University, Beijing 100875, China*

²*The Key Laboratory of Weak Light Nonlinear Photonics, Ministry of Education, Teda
Applied Physics Institute and School of Physics, Nankai University, Tianjin 300457, China*

³*Institute of Physics, Chinese Academy of Sciences, Beijing 100190, China*

⁴*School of Physical Sciences, University of Chinese Academy of Sciences, Beijing 100190,
China*

⁵*Theoretical Quantum Physics Laboratory, RIKEN Cluster for Pioneering Research,
Wako-shi, Saitama 351-0198, Japan*

⁶*CAS Center for Excellence in Topological Quantum Computation, University of Chinese
Academy of Sciences, Beijing 100190, China*

⁷*School of Physics, Northwest University, Xi'an 710127, China*

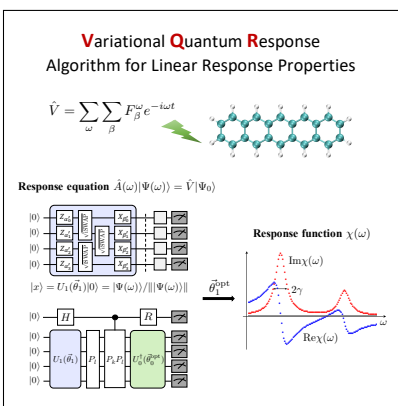
Contributed equally to this work

* E-mail: kaixu@iphy.ac.cn; liuzb@nankai.edu.cn; zhendongli@bnu.edu.cn; hfan@iphy.ac.cn

Abstract

Simulating response properties of molecules is crucial for interpreting experimental spectroscopies and accelerating materials design. However, it remains a long-standing computational challenge for electronic structure methods on classical computers. While quantum computers hold the promise to solve this problem more efficiently in the long run, existing quantum algorithms requiring deep quantum circuits are infeasible for near-term noisy quantum processors. Here, we introduce a pragmatic variational quantum response (VQR) algorithm for response properties, which circumvents the need for deep quantum circuits. Using this algorithm, we report the first simulation of linear response properties of molecules including dynamic polarizabilities and absorption spectra on a superconducting quantum processor. Our results indicate that a large class of important dynamical properties such as Green’s functions are within the reach of near-term quantum hardware using this algorithm in combination with suitable error mitigation techniques.

Graphical TOC Entry



In silico simulation of molecular response properties, such as dynamic polarizabilities, absorption/emission spectra, and nonlinear optical properties, is essential in virtual design of new materials with specific properties.¹ However, despite decades of effort and tremendous progress in methodological developments, their accurate and efficient prediction remains a fundamental challenge for electronic structure methods on classical computers.^{2,3} On one hand, while density functional theory (DFT) and its time-dependent extension (TD-DFT) have been the workhorse for simulating structural and response properties of large molecules due to their good efficiency, the limitations of density functional approximations are well-known,⁴ especially for strongly correlated systems. On the other hand, the exact method for solving the many-electron Schrödinger equation within a given basis set, namely, full configuration interaction (FCI) or exact diagonalization,² has an exponential scaling with respect to the system size in both physical memory and computational time.

Quantum computing is promising for simulating interacting many-body systems including molecules.⁵⁻⁸ So far, quantum simulations of molecules on the present noisy intermediate-scale quantum (NISQ)⁹ devices have almost exclusively focused on the ground state $|\Psi_0\rangle$ and the associated energy E_0 ,¹⁰⁻¹⁵ which is the very first step towards simulating molecular properties. Computing (frequency-dependent) linear and nonlinear response properties is far more challenging, because they implicitly involve not only the ground state but also all the excited states.³ While it is possible to compute response properties using the sum-over-state formula (see Eq. (1)) with individual excited state computed by existing quantum algorithms,¹⁶⁻²¹ such approach will quickly become impractical as the number of excited states grows exponentially with the system size. Previous quantum algorithms for linear response functions largely rely on computing time-correlation functions using quantum computers,²²⁻²⁵ which can later be Fourier transformed to the frequency domain on classical computers. Very recently, they have been realized for spin- $\frac{1}{2}$ Heisenberg models (with up to four sites) on superconducting quantum processors.²³⁻²⁵ However, as implementing the time evolution operator $e^{-i\hat{H}_0 t}$ with the molecular Hamiltonian \hat{H}_0 requires a formidably large

circuit depth, which at least scales as $O(n^4)$ with respect to the number of qubits n ^{26–28} or $O(n^2)$ with low-rank approximations²⁹ asymptotically, it is difficult to apply these algorithms for molecules on NISQ devices. Thus, how to compute molecular response properties on near-term quantum hardware remains an open problem.

In this Letter, we describe a pragmatic quantum computational approach for computing linear response properties, which circumvents the need for deep quantum circuits. Specifically, we propose efficient quantum circuits to solve the frequency-domain linear response equation in a variational hybrid quantum-classical way. Together with an error mitigation (EM) strategy based on symmetry projection to mitigate the impact of noises inherent in NISQ devices, we realize the first simulation of linear response properties of molecules including dynamic polarizabilities and absorption spectra on a programmable superconducting quantum processor.³⁰ The present approach can be easily extended to simulate other important dynamical properties such as Green’s functions and nonlinear response properties, and is also applicable to other platforms such as trapped-ion systems.^{13,31}

Variational quantum response (VQR) algorithm. We consider the computation of the following linear response function, which characterizes the first order response of molecules to an applied external field

$$\chi(\omega) = \sum_m \frac{|\langle \Psi_m | \hat{V} | \Psi_0 \rangle|^2}{\omega_{m0} - (\omega + i\gamma)}, \quad (1)$$

where ω represents the frequency of the external field and the parameter γ determines the frequency resolution, which is usually adjusted to best fit an experimental spectrum of molecules.³ Depending on the perturbation \hat{V} , $\chi(\omega)$ can be dynamic polarizabilities, magnetic susceptibilities, Green’s functions, etc. It encodes all the information of the excitation process from the ground state $|\Psi_0\rangle$ to the m -th excited state $|\Psi_m\rangle$ due to the perturbation \hat{V} , viz., the excitation energy $\omega_{m0} = E_m - E_0$ and the transition amplitude $|\langle \Psi_m | \hat{V} | \Psi_0 \rangle|^2$. Exact calculations of $\chi(\omega)$ on classical computers are generally intractable, as the number of

excited states scales exponentially with the molecular size.² To compute $\chi(\omega)$ on quantum computers, an appropriate fermion-to-qubit mapping^{27,32} is first applied to transform \hat{H}_0 and \hat{V} for electrons to their counterparts for n qubits, i.e., $\hat{H}_0 = \sum_k h_k P_k$ and $\hat{V} = \sum_k v_k P_k$, which are linear combinations of Pauli terms $P_k = \sigma_0^k \otimes \sigma_1^k \otimes \dots \otimes \sigma_{n-1}^k$ with $\sigma_i \in \{I, X, Y, Z\}$. For spin models with a much simpler \hat{H}_0 , previous quantum algorithms²²⁻²⁵ computed the dynamical correlation function $C(t) = \langle \Psi_0 | \hat{V}^\dagger(t) \hat{V} | \Psi_0 \rangle = \sum_{lk} v_l v_k \langle \Psi_0 | P_l(t) P_k | \Psi_0 \rangle$ with $P_l(t) = e^{i\hat{H}_0 t} P_l e^{-i\hat{H}_0 t}$ using the quantum circuit for $\langle \Psi_0 | P_l(t) P_k | \Psi_0 \rangle$ shown in Fig. 1a repeatedly for different time t , and then performed a Fourier transform to obtain $\chi(\omega)$. However, as the number of Pauli terms in \hat{H}_0 scales as $O(n^4)$ for molecules, implementing $e^{-i\hat{H}_0 t}$ requires a large circuit depth, which at least scales as $O(n^4)$ ²⁶⁻²⁸ or $O(n^2)$ with low-rank approximations²⁹ asymptotically, which makes the application of these algorithms to molecules on near-term quantum hardware very challenging.

To overcome this difficulty, we adopt the frequency-domain formulation for response properties,³³⁻³⁵ which avoids the formidable sum over all excited states in Eq. (1) by introducing an auxiliary response state $|\Psi(\omega)\rangle$ satisfying

$$\hat{A}(\omega)|\Psi(\omega)\rangle = \hat{V}|\Psi_0\rangle, \quad \hat{A}(\omega) = \hat{H}_0 - E_0 - (\omega + i\gamma), \quad (2)$$

such that $\chi(\omega)$ becomes a simple expectation value $\chi(\omega) = \langle \Psi(\omega) | \hat{A}^\dagger(\omega) | \Psi(\omega) \rangle$ similar to the energy $E_0 = \langle \Psi_0 | \hat{H}_0 | \Psi_0 \rangle$. It has been shown that using the Harrow-Hassidim-Lloyd (HHL) algorithm³⁶ or its improvements³⁷⁻³⁹ to solve the linear response equation (2) can offer an exponential speedup³³ over classical FCI-based response algorithms,² provided the ground state $|\Psi_0\rangle$ has been prepared on quantum computers. However, realizing these quantum algorithms faces the same difficulty as implementing the time evolution on NISQ devices. Following the variational hybrid quantum-classical algorithm for linear system of equations,^{40,41} we present a pragmatic algorithmic primitive for solving Eq. (2), which can also be extended to high-order response equations for nonlinear response properties. Suppose the ground state

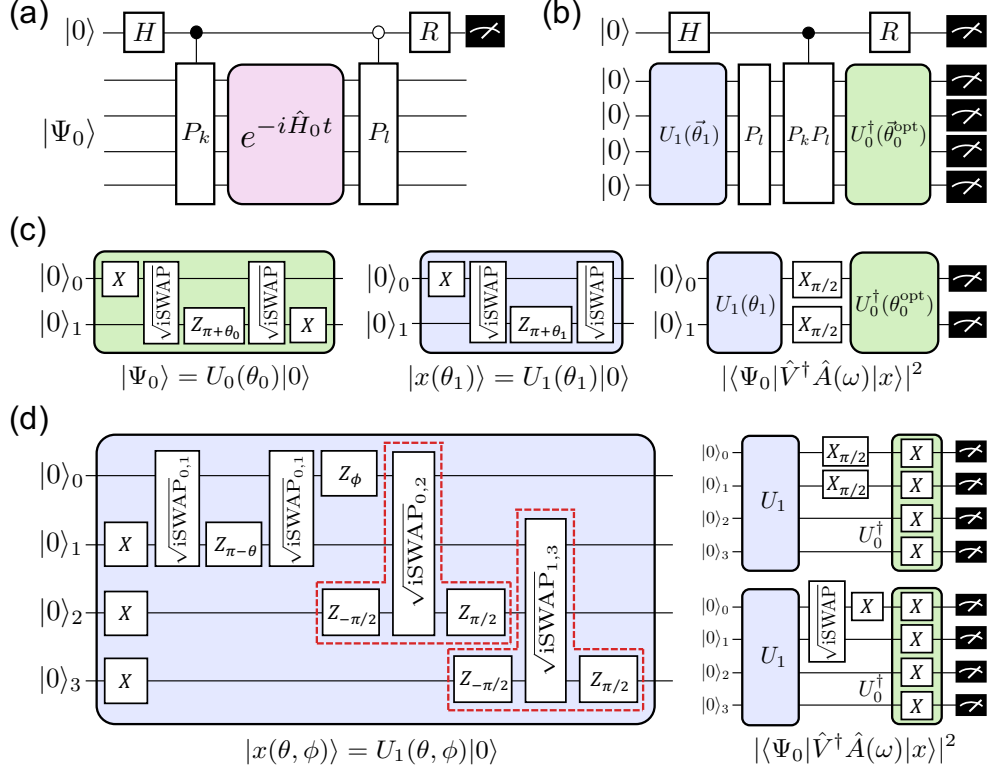


Figure 1: Quantum computation of linear response functions $\chi(\omega)$. (a) Quantum circuit for computing the dynamical correlation function $\langle\Psi_0|P_l(t)P_k|\Psi_0\rangle$ where R is the Hadamard gate H (or $X_{\pi/2}$) for computing the real (or imaginary) part. (b) Quantum circuit for computing $\langle x|P_l|\Psi_0\rangle\langle\Psi_0|P_k|x\rangle$ with $|\Psi_0\rangle = U_0|0\rangle$ and $|x\rangle = U_1|0\rangle$. (c) Two-qubit simulations of H_2 and polyacenes: PQCs for $|\Psi_0\rangle$ and $|x\rangle$ as well as the quantum circuit for computing $|\langle\Psi_0|\hat{V}^\dagger\hat{A}(\omega)|x\rangle|^2$ (d) Four-qubit simulations of CO: PQC for $|x\rangle$ and the two quantum circuits for computing $|\langle\Psi_0|\hat{V}^\dagger\hat{A}(\omega)|x\rangle|^2$. The red dashed box represents the entangling gate generating a spin singlet pair $\frac{1}{\sqrt{2}}(|01\rangle + |10\rangle)$ between the two qubits.

has been prepared by $|\Psi_0\rangle = U_0(\vec{\theta}_0^{\text{opt}})|0\rangle$, where $U_0(\vec{\theta}_0)$ is a parameterized quantum circuit (PQC) with a set of free angles $\vec{\theta}_0$ whose optimal values can be determined using the variational quantum eigensolver (VQE).^{10,42} To solve Eq. (2), one can design a PQC $U_1(\vec{\theta}_1)$ for the normalized response state at a given frequency $|x\rangle \equiv |\Psi(\omega)\rangle/||\Psi(\omega)\rangle|| = U_1(\vec{\theta}_1)|0\rangle$, and then find the optimal parameters $\vec{\theta}_1^{\text{opt}}$ by minimizing a cost function constructed using the Cauchy-Schwarz inequality

$$L(\vec{\theta}_1) = \langle\Psi_0|\hat{V}^\dagger\hat{V}|\Psi_0\rangle\langle x|\hat{A}^\dagger(\omega)\hat{A}(\omega)|x\rangle - |\langle\Psi_0|\hat{V}^\dagger\hat{A}(\omega)|x\rangle|^2, \quad (3)$$

which obeys $L(\vec{\theta}_1) \geq 0$. Its minimum is uniquely achieved at $|x\rangle \propto \hat{A}^{-1}(\omega)\hat{V}|\Psi_0\rangle$ for the nonsingular operator $\hat{A}(\omega)$. Note that the choice of cost functions for solving Eq. (2) is not unique,^{40,41} and our choice has the advantage that the squared cross term $|\langle\Psi_0|\hat{V}^\dagger\hat{A}(\omega)|x\rangle|^2$ can be computed with less controlled operations (vide post), which are more friendly for NISQ devices. With $\vec{\theta}_1^{\text{opt}}$ obtained at a given frequency, $\chi(\omega)$ can be computed from (see Supporting Information⁴³)

$$\chi(\omega) = \langle x|\hat{A}^\dagger(\omega)|x\rangle \frac{\langle\Psi_0|\hat{V}^\dagger\hat{V}|\Psi_0\rangle}{\langle x|\hat{A}^\dagger(\omega)\hat{A}(\omega)|x\rangle}. \quad (4)$$

The expectation values in Eqs. (3) and (4), i.e., $\langle\Psi_0|\hat{V}^\dagger\hat{V}|\Psi_0\rangle$, $\langle x|\hat{A}^\dagger(\omega)\hat{A}(\omega)|x\rangle$, and $\langle x|\hat{A}^\dagger(\omega)|x\rangle$, can be simply computed by measurements after preparing $|\Psi_0\rangle$ or $|x\rangle$ on quantum computers. The computation of $|\langle\Psi_0|\hat{V}^\dagger\hat{A}(\omega)|x\rangle|^2$ in Eq. (3) is more involved. Using the expansion $\hat{V}^\dagger\hat{A}(\omega) = \sum_k c_k(\omega)P_k$ derivable from the expansions for \hat{V} and \hat{H}_0 , $|\langle\Psi_0|\hat{V}^\dagger\hat{A}(\omega)|x\rangle|^2$ becomes $\sum_{lk} \bar{c}_l(\omega)c_k(\omega)\langle x|P_l|\Psi_0\rangle\langle\Psi_0|P_k|x\rangle$. We introduce a quantum circuit for computing $\langle x|P_l|\Psi_0\rangle\langle\Psi_0|P_k|x\rangle$ with an ancilla qubit (Fig. 1b), whose depth is dominated by the sum of depths for $U_0(\vec{\theta}_0^{\text{opt}})$ and $U_1(\vec{\theta}_1)$. Unlike previous works using the Hadamard test,^{40,41} this scheme does not require any controlled operation on $U_0(\vec{\theta}_0^{\text{opt}})$ nor $U_1(\vec{\theta}_1)$. Moreover, for certain problems with symmetries, the computation of $|\langle\Psi_0|\hat{V}^\dagger\hat{A}(\omega)|x\rangle|^2$ can be further simplified to quantum circuits without the ancilla (see Figs. 1c and 1d as well as Supporting Information⁴³ for details). With low-depth ansätze¹² for $U_0(\vec{\theta}_0)$ and $U_1(\vec{\theta}_1)$, the present algorithm is more feasible on near-term quantum hardware than existing quantum algorithms for response properties.²²⁻²⁵

The present algorithm adds two new contributions to the arsenal of quantum computational chemistry.⁵⁻⁸ First, the unique feature of VQR is that it enables the computation of linear response properties directly in a frequency region of interest. The calculations for different frequencies are completely independent and hence can be carried out in parallel. Second, as a method for simulating excitation spectra, VQR is more advantageous than

quantum algorithms solely for excited states^{16–21} in several aspects. It not only gives peak positions, but also provides relative transition strengths simultaneously. Besides, in the frequency region with a large density of states, performing the slowly convergent sum in Eq. (1) by computing excited states is cumbersome, and the implicit sum using VQR is more elegant.

Hardware implementation and error mitigation. With the VQR algorithm, we are able to perform the first quantum simulation of linear response properties of molecules on a superconducting processor, including dynamic polarizabilities of the hydrogen molecule (H_2), ultraviolet-visible (UV-Vis) absorption spectra of polyacenes, and X-ray absorption spectra of carbon monoxide (CO). In these cases, \hat{V} is a dipole operator (\hat{x} , \hat{y} , or \hat{z}), such that $\chi(\omega)$ represents the resonant contribution to dipole polarizability, whose imaginary part is related with the linear absorption of radiation $\sigma_{\text{abs}}(\omega)$ by a randomly oriented molecular sample in the electric-dipole approximation,³ viz., $\sigma_{\text{abs}}(\omega) = \frac{4\pi\omega}{c} \text{Im}\bar{\chi}(\omega)$ with $\bar{\chi} = \frac{1}{3}(\chi_{xx} + \chi_{yy} + \chi_{zz})$ and c being the speed of light. The lineshape of $\sigma_{\text{abs}}(\omega)$ can be understood by noting that $\text{Im}\chi(\omega) = \gamma \frac{\langle \Psi_0 | \hat{V}^\dagger \hat{V} | \Psi_0 \rangle}{\langle x | \hat{A}^\dagger(\omega) \hat{A}(\omega) | x \rangle} = \sum_m |\langle \Psi_m | \hat{V} | \Psi_0 \rangle|^2 \frac{\gamma}{(\omega_{m0} - \omega)^2 + \gamma^2}$ is a weighted superposition of Lorentzians with a common full width at half maximum (FWHM) 2γ .

The superconducting quantum processor³⁰ used in our simulations consists of 20 frequency-tunable transmon qubits connected via a central resonator, which was employed before for realizing quantum generative adversarial networks⁴⁴ and characterizing multiparticle entangled states.⁴⁵ A special feature of this device is that the $\sqrt{\text{iSWAP}}_{i,j}$ gate can be realized between any pair of qubits. The fidelity characterized by quantum process tomography^{46,47} is 0.9806 for the $\sqrt{\text{iSWAP}}$ gate in the simulations of H_2 and polyacenes with circuits shown in Fig. 1c, while the average fidelity for the three $\sqrt{\text{iSWAP}}$ gates in the simulations of CO with circuits shown in Fig. 1d is slightly lower (ca. 0.9651). More detailed information about the device and experimental setup can be found in Supporting Information.⁴³

Since we mainly focus on the feasibility of VQR on NISQ devices in this work, we employ PQCs capable of encoding the exact ground or response state as variational ansätze,

and perform numerical optimizations by scanning the entire parameter space (instead of using a classical optimizer). To mitigate the impact of noises, we employ a simple EM strategy based on symmetry projection for expectation values in VQE/VQR, which is similar to the EM strategy by symmetry verification.^{14,48} Specifically, to improve the estimate of $\langle \Psi | \hat{O} | \Psi \rangle$ for a quantum state $|\Psi\rangle$ with certain symmetry and an operator \hat{O} (e.g., \hat{H}_0 , $\hat{A}(\omega)$, $\hat{A}^\dagger(\omega)\hat{A}(\omega)$, and $\hat{V}^\dagger\hat{V}$) commuting with the associated symmetry projector \mathcal{P} (viz., $\mathcal{P}|\Psi\rangle = |\Psi\rangle$ and $[\hat{O}, \mathcal{P}] = 0$), instead of using the raw result $\langle \Psi | \hat{O} | \Psi \rangle^{\text{raw}} \equiv \text{tr}(\rho_{\text{exp}}\hat{O})$, we can use $\langle \Psi | \hat{O} | \Psi \rangle^{\text{EM}} \equiv \text{tr}(\rho_{\text{proj}}\hat{O}) = \text{tr}(\mathcal{P}\rho_{\text{exp}}\mathcal{P}\hat{O})/\text{tr}(\rho_{\text{exp}}\mathcal{P}) = \text{tr}(\rho_{\text{exp}}\hat{O}\mathcal{P})/\text{tr}(\rho_{\text{exp}}\mathcal{P})$, where $\text{tr}(\rho_{\text{exp}}\hat{O}\mathcal{P})$ and $\text{tr}(\rho_{\text{exp}}\mathcal{P})$ need to be measured on quantum computers and $\rho_{\text{proj}} = \mathcal{P}\rho_{\text{exp}}\mathcal{P}/\text{tr}(\rho_{\text{exp}}\mathcal{P})$ is the symmetry-projected density matrix with unphysical components outside the correct subspace due to noises removed via symmetry projection. The specific form of \mathcal{P} for each molecule can be found in Supporting Information.⁴³ The use of EM is found essential for the accuracy of the simulated spectra, since the demoninator $\langle x | \hat{A}^\dagger(\omega)\hat{A}(\omega) | x \rangle$ in Eq. (4) is crucial for determining peak positions and heights.

Results. Due to its conceptual simplicity, H₂ in a minimal basis set has become a test bed for new quantum algorithms.^{10-14,49} We compute its dipole polarizability for $\hat{V} = \hat{z}$ and $\gamma = 0.1$ a.u. using VQR at three representative bond distances, viz., $R = R_e$ (the equilibrium bond length⁵⁰), $2R_e$, and $3R_e$, which cover the weak, intermediate, and strong electron correlation regimes. Figure 2 displays the ground-state energies and dynamic polarizabilities obtained by VQE and VQR, respectively, using the quantum circuits shown in Fig. 1c. In both VQE and VQR, EM with a spatial symmetry projector leads to a better agreement with the corresponding FCI values than the raw results. This is particular the case for the peaks of $\text{Im}\chi(\omega)$ predicted by VQR for the transition from the ground state $|^1\Psi_g\rangle$ to the first singlet excited states $|^1\Psi_u\rangle$. Meanwhile, small deviations from the FCI curves are observed for $\chi(\omega)$ at ω around 0.6, 0.1, and 0.0 a.u. for $R = R_e$, $2R_e$, and $3R_e$, respectively. These frequencies turn out to be exactly the position of the first triplet excited state $|^3\Psi_u\rangle$ at each geometry (see Supporting Information⁴³). Around these regions, the two terms in $L(\theta_1)$ are very

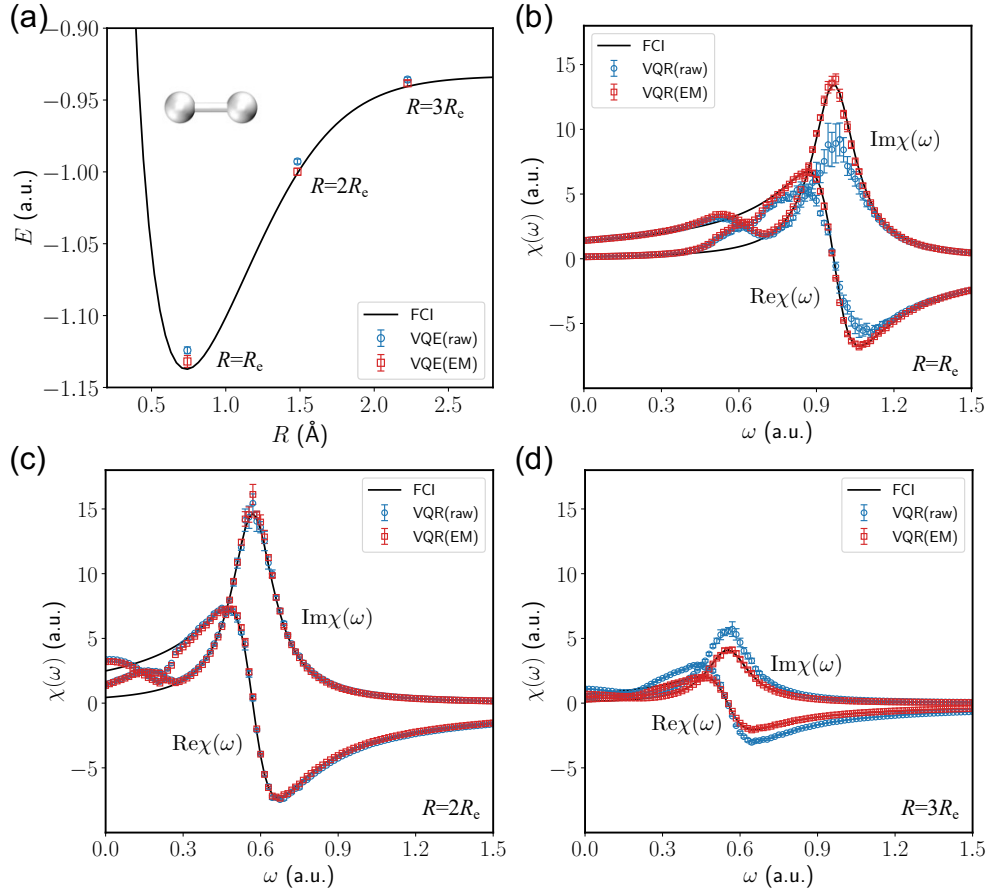


Figure 2: Ground-state energies and dynamic polarizabilities of H₂ at three representative bond distances from two-qubit simulations. (a) Ground-state energies computed using VQE without (blue) and with EM (red). (b),(c),(d) Real and imaginary parts of dipole polarizability $\chi(\omega)$ for $\hat{V} = \hat{z}$ and $\gamma = 0.1$ a.u. computed using VQR without (blue) and with EM (red) at different bond distances.

close to each other and the difference is on the order of γ^2 . Consequently, the computation of $L(\theta_1)$ is prone to noises on each term, such that the optimized angle θ_1^{opt} becomes less accurate. Improving the two-qubit gate fidelity will alleviate this problem (see Supporting Information⁴³), and further applying a spin symmetry projector to filter out triplet states will completely remove the small spurious speaks in $\text{Im}\chi(\omega)$. Comparison with $\chi(\omega)$ computed using the Hartree-Fock method and DFT with some popular exchange-correlation functionals (see Supporting Information⁴³) reveals the limitation of these approximate methods in the strong correlation regime, for which VQR may become a better computational tool in future.

Next, we examine the potential of VQR in solving important realistic problems. We ap-

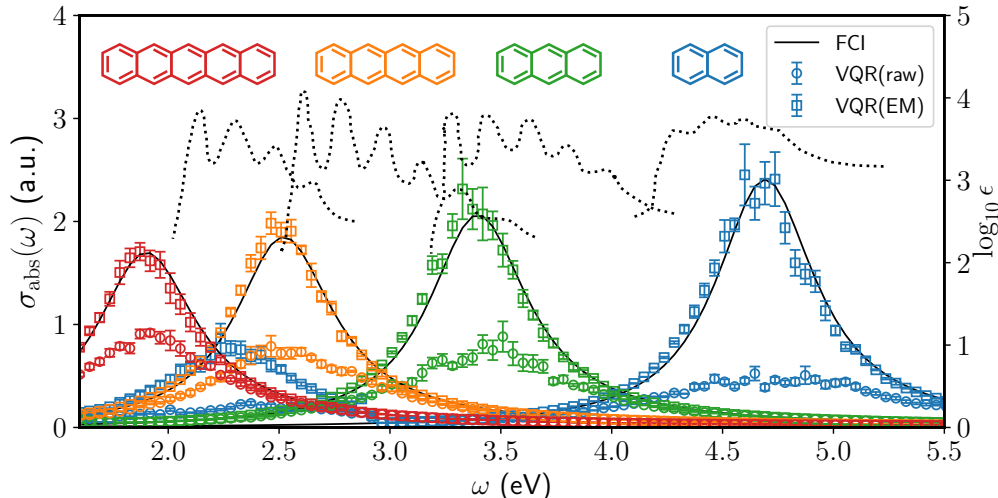


Figure 3: UV-Vis absorption spectra $\sigma_{\text{abs}}(\omega)$ ($\gamma = 0.01$ a.u.) from two-qubit simulations using VQR for polyacenes. Experimental absorption spectra⁵¹ (dotted lines) are shown for comparison. All the computed spectra have been shifted by -1.9 eV estimated using perturbation theory for dynamic electron correlation (see Supporting Information⁴³).

ply VQR to simulate the first absorption band (the so-called 1L_a or p band⁵¹) of polyacenes due to the transition from the highest occupied molecular orbital (HOMO) to the lowest unoccupied molecular orbital (LUMO), which is the most relevant band for their applications as optoelectronic devices.⁵² As qubit resources are currently quite limited, simulating the entire molecule remains impossible for polyacenes. Thus, we combine VQR with the complete active space (CAS) model,⁵³ in which only a selected number of electrons and orbitals are treated at the FCI level. Figure 3 shows the computed UV-Vis absorption spectra $\sigma_{\text{abs}}(\omega)$ for polyacenes (including naphthalene, anthracene, tetracene, and pentacene) using a minimal active space composed of HOMO and LUMO with two active electrons, denoted by CAS(2e,2o). The same quantum circuits (Fig. 1c) as for H_2 are used in VQE and VQR for the reduced active-space problems, but a smaller γ (0.01 a.u.) is used for a better resolution in the UV-Vis region. Compared with the VQR(raw) results for H_2 , the VQR(raw) results here show less good agreement with the FCI references, because the computation of the denominator $\langle x | \hat{A}^\dagger(\omega) \hat{A}(\omega) | x \rangle$ in Eq. (4) is more sensitive to noises for smaller γ . Even in this case, the VQR(EM) spectra agree well with the FCI spectra, except for the appearance

of a small spurious peak around 2.3 eV for naphthalene due to the same problem found for H_2 . Compared with the experimental spectra of polyacenes,⁵¹ our simulations successfully reproduce the remarkable red shift as the number of rings increases. To have a better quantitative agreement, dynamic electron correlation and vibronic couplings need to be taken into account in future. Although not illustrated in this work, we mention that the VQR algorithm is also applicable to simulating emission spectra, provided the initial excited state is prepared on quantum computers, e.g., using the variational quantum deflation method.¹⁸

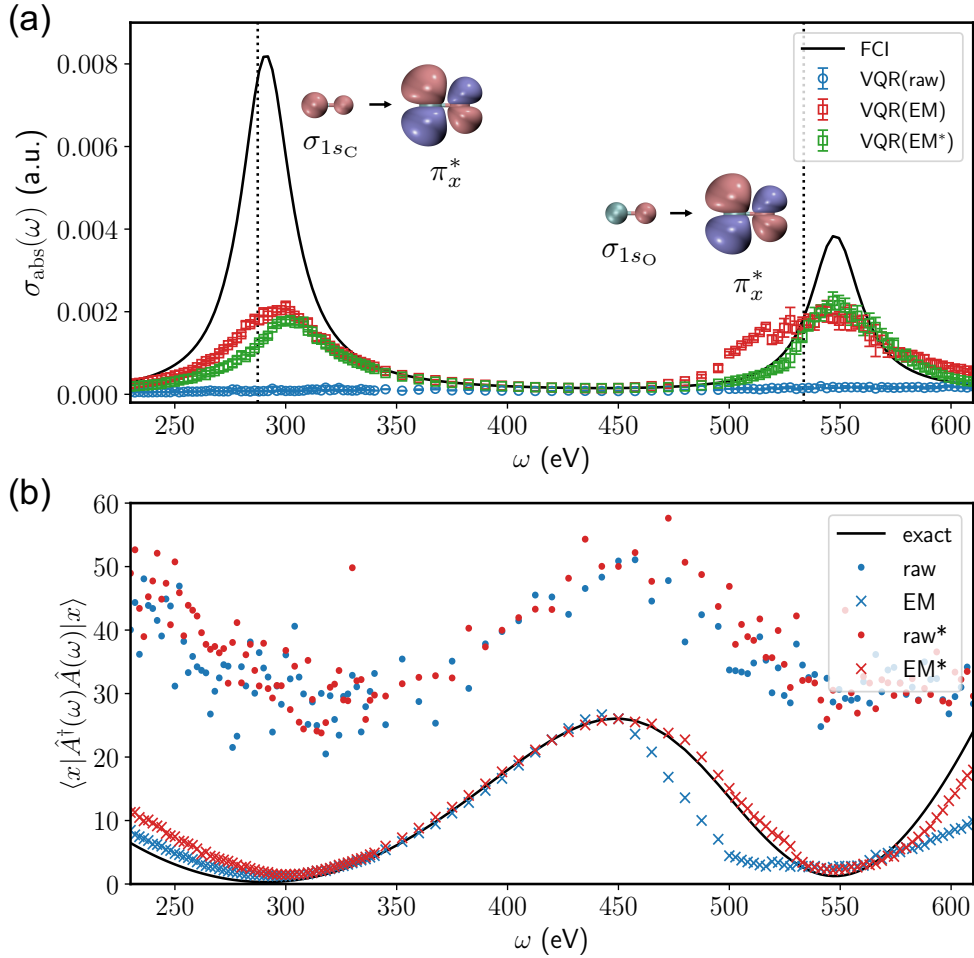


Figure 4: X-ray absorption spectra of CO from four-qubit simulations. (a) Simulated spectra $\sigma_{\text{abs}}(\omega)$ ($\hat{V} = \hat{x}$ and $\gamma = 0.5$ a.u.) using VQR. VQR(EM*) represents the spectrum measured at the theoretical angles (θ^*, ϕ^*) at each frequency. Experimental core excitation energies^{54,55} (vertical dotted lines) are shown for comparison. (b) Results for $\langle x | \hat{A}^\dagger(\omega) \hat{A}(\omega) | x \rangle$ using the experimentally optimized $(\theta^{\text{opt}}, \phi^{\text{opt}})$ (labelled by raw and EM) and the theoretical (θ^*, ϕ^*) (labelled by raw* and EM*) at each frequency, compared against the exact curve (black line).

Finally, we apply VQR to simulate X-ray spectroscopies, which are widely utilized for probing local molecular and electronic structures, but remain challenging for theoretical prediction.^{56,57} The carbon K-edge and oxygen K-edge absorption spectra of CO are simulated using VQR with a CAS(4e,3o) model composed of σ_{1s_O} , σ_{1s_C} , and π_x^* orbitals. The ground state is well-approximated by the Hartree-Fock state, $|\Psi_0\rangle = U_0|0\rangle$ with $U_0 = X_0X_1X_2X_3$. For $\hat{V} = \hat{x}$, a response state can be exactly parameterized by $|x(\theta, \phi)\rangle = U_1(\theta, \phi)|0\rangle = \cos\frac{\theta}{2}|^1\Psi_{\sigma_{1s_O}\rightarrow\pi_x^*}\rangle + \sin\frac{\theta}{2}e^{i\phi}|^1\Psi_{\sigma_{1s_C}\rightarrow\pi_x^*}\rangle$ with two free angles θ and ϕ , where $U_1(\theta, \phi)$ is the PQC in Fig. 1d and $|^1\Psi_{\sigma_{1s_O}\rightarrow\pi_x^*}\rangle$ ($|^1\Psi_{\sigma_{1s_C}\rightarrow\pi_x^*}\rangle$) represents the singlet excited state due to the transition from the core orbital σ_{1s_O} (σ_{1s_C}) to the unoccupied orbital π_x^* . Figure 4a displays the simulated spectra $\sigma_{\text{abs}}(\omega)$ using VQR. It is clear that the improvement by EM is essential. While the VQR(raw) spectrum is almost vanishing, the VQR(EM) spectrum has two obvious absorption peaks. Compared with the previous two-qubit simulations, the deviation of the VQR(EM) spectrum from the FCI reference is larger for peak heights. To better understand this discrepancy, we also measure the spectra using the theoretical angles (θ^*, ϕ^*) for $L(\theta, \phi)$ at each frequency (denoted by VQR(EM*) in Fig. 4a), and compare the corresponding values of $\langle x|\hat{A}^\dagger(\omega)\hat{A}(\omega)|x\rangle$ in Eq. (4) obtained using the experimentally optimized $(\theta^{\text{opt}}, \phi^{\text{opt}})$ and the theoretical angles (see Fig. 4b). This comparison reveals that the deviation in peak heights is not dominated by errors in the optimization of $L(\theta, \phi)$, but is mainly due to errors in computing $\langle x|\hat{A}^\dagger(\omega)\hat{A}(\omega)|x\rangle$ arising from experimental imperfections such as the lowering of two-qubit gate fidelities in realizing the quantum circuit for $|x(\theta, \phi)\rangle$ (Fig. 1d). Therefore, a further reduction of the deviation can be anticipated using better quantum hardware with higher two-qubit gate fidelities or more sophisticated EM strategies developed for VQE⁵⁸ in computing $\langle x|\hat{A}^\dagger(\omega)\hat{A}(\omega)|x\rangle$. Note that even though the peak heights in the present VQR(EM) calculations are not ideal, the core excitation energies for $|^1\Psi_{\sigma_{1s_O}\rightarrow\pi_x^*}\rangle$ and $|^1\Psi_{\sigma_{1s_C}\rightarrow\pi_x^*}\rangle$ determined by the peak positions are still reasonably good. The remaining discrepancy with the experimental core excitation energies obtained from high-resolution photoabsorption spectra^{54,55} can be improved by employing a larger active

space and a better basis set in future.

Conclusion. We introduced a quantum algorithm feasible on near-term quantum hardware for computing molecular linear response properties. While the reported experimental results are not perfect due to the presence of noises, the validity and feasibility of the VQR algorithm are clearly demonstrated. The results highlight that it is the combination of three key innovations, i.e., frequency-domain formulation for response properties, variational algorithms for linear response equation with low-depth quantum circuits, and error mitigation techniques, that makes the simulation of molecular linear response properties possible on NISQ devices for the first time. This work suggests that a large class of important dynamical response properties such as emission spectra, Green’s functions, and nonlinear optical properties are accessible on near-term quantum hardware using the VQR approach. Moreover, the present approach is not limited to superconducting devices, but is also applicable to other quantum computing platforms. Many improvements from different aspects can be easily envisaged, such as lowering the number of measurements, employing better EM techniques, using quantum gradients in optimizations,⁴⁴ as well as improving quantum hardware. Therefore, we believe that the present algorithm opens the door for applying quantum computing for simulating static and dynamical response properties of more complex molecules and condense-phase systems in future.

Acknowledgement

This work was supported by the National Natural Science Foundation of China (Grant Nos. 21973003, 21688102, T2121001, 11934018, 11904393, 92065114 and 12174207), the Strategic Priority Research Program of Chinese Academy of Sciences (Grant No. XDB28000000) and the Beijing Natural Science Foundation (Grant No. Z200009).

Supporting Information Available

Additional theoretical derivations, algorithms for the cross term, and experimental details including device information, two-qubit simulations for H₂ and polyacenes, and four-qubit simulations for CO.

References

- (1) Marzari, N.; Ferretti, A.; Wolverton, C. Electronic-structure methods for materials design. *Nat. Mater.* **2021**, *20*, 736–749.
- (2) Helgaker, T.; Coriani, S.; Jørgensen, P.; Kristensen, K.; Olsen, J.; Ruud, K. Recent advances in wave function-based methods of molecular-property calculations. *Chem. Rev.* **2012**, *112*, 543–631.
- (3) Norman, P.; Ruud, K.; Saue, T. *Principles and practices of molecular properties: Theory, modeling, and simulations*; John Wiley & Sons, 2018.
- (4) Cohen, A. J.; Mori-Sánchez, P.; Yang, W. Insights into current limitations of density functional theory. *Science* **2008**, *321*, 792–794.
- (5) Cao, Y.; Romero, J.; Olson, J. P.; Degroote, M.; Johnson, P. D.; Kieferová, M.; Kivlichan, I. D.; Menke, T.; Peropadre, B.; Sawaya, N. P.; Sim, S.; Veis, L.; Aspuru-Guzik, A. Quantum chemistry in the age of quantum computing. *Chem. Rev.* **2019**, *119*, 10856–10915.
- (6) McArdle, S.; Endo, S.; Aspuru-Guzik, A.; Benjamin, S. C.; Yuan, X. Quantum computational chemistry. *Rev. Mod. Phys.* **2020**, *92*, 015003.
- (7) Bauer, B.; Bravyi, S.; Motta, M.; Chan, G. K.-L. Quantum algorithms for quantum chemistry and quantum materials science. *Chem. Rev.* **2020**, *120*, 12685–12717.

- (8) Motta, M.; Rice, J. E. Emerging quantum computing algorithms for quantum chemistry. *Wiley Interdiscip. Rev. Comput. Mol. Sci.* **2021**, e1580.
- (9) Preskill, J. Quantum Computing in the NISQ era and beyond. *Quantum* **2018**, *2*, 79.
- (10) Peruzzo, A.; McClean, J.; Shadbolt, P.; Yung, M.-H.; Zhou, X.-Q.; Love, P. J.; Aspuru-Guzik, A.; O'Brien, J. L. A variational eigenvalue solver on a photonic quantum processor. *Nat. Commun.* **2014**, *5*, 4213.
- (11) O'Malley, P. J. J.; Babbush, R.; Kivlichan, I. D.; Romero, J.; McClean, J. R.; Barends, R.; Kelly, J.; Roushan, P.; Tranter, A.; Ding, N.; Campbell, B.; Chen, Y.; Chen, Z.; Chiaro, B.; Dunsworth, A.; Fowler, A. G.; Jeffrey, E.; Lucero, E.; Megrant, A.; Mutus, J. Y.; Neeley, M.; Neill, C.; Quintana, C.; Sank, D.; Vainsencher, A.; Wenner, J.; White, T. C.; Coveney, P. V.; Love, P. J.; Neven, H.; Aspuru-Guzik, A.; Martinis, J. M. Scalable quantum simulation of molecular energies. *Phys. Rev. X* **2016**, *6*, 031007.
- (12) Kandala, A.; Mezzacapo, A.; Temme, K.; Takita, M.; Brink, M.; Chow, J. M.; Gambetta, J. M. Hardware-efficient variational quantum eigensolver for small molecules and quantum magnets. *Nature* **2017**, *549*, 242.
- (13) Hempel, C.; Maier, C.; Romero, J.; McClean, J.; Monz, T.; Shen, H.; Jurcevic, P.; Lanyon, B. P.; Love, P.; Babbush, R.; Aspuru-Guzik, A.; Blatt, R.; Roos, C. F. Quantum chemistry calculations on a trapped-ion quantum simulator. *Phys. Rev. X* **2018**, *8*, 031022.
- (14) Sagastizabal, R.; Bonet-Monroig, X.; Singh, M.; Rol, M. A.; Bultink, C.; Fu, X.; Price, C.; Ostroukh, V.; Muthusubramanian, N.; Bruno, A.; Beekman, M.; Haider, N.; O'Brien, T. E.; DiCarlo, L. Experimental error mitigation via symmetry verification in a variational quantum eigensolver. *Phys. Rev. A* **2019**, *100*, 010302.
- (15) Arute, F.; Arya, K.; Babbush, R.; Bacon, D.; Bardin, J. C.; Barends, R.; Boixo, S.; Broughton, M.; Buckley, B. B.; Buell, D. A.; Burkett, B.; Bushnell, N.; Chen, Y.;

- Chen, Z.; Chiaro, B.; Collins, R.; Courtney, W.; Demura, S.; Dunsworth, A.; Farhi, E.; Fowler, A.; Foxen, B.; Gidney, C.; Giustina, M.; Graff, R.; Habegger, S.; Harri- gan, M. P.; Ho, A.; Hong, S.; Huang, T.; Huggins, W. J.; Ioffe, L.; Isakov, S. V.; Jef- frey, E.; Jiang, Z.; Jones, C.; Kafri, D.; Kechedzhi, K.; Kelly, J.; Kim, S.; Klimov, P. V.; Korotkov, A.; Kostritsa, F.; Landhuis, D.; Laptev, P.; Lindmark, M.; Lucero, E.; Martin, O.; Martinis, J. M.; McClean, J. R.; McEwen, M.; Megrant, A.; Mi, X.; Mohseni, M.; Mruczkiewicz, W.; Mutus, J.; Naaman, O.; Neeley, M.; Neill, C.; Neven, H.; Niu, M. Y.; O’Brien, T. E.; Ostby, E.; Petukhov, A.; Putterman, H.; Quin- tana, C.; Roushan, P.; Rubin, N. C.; Sank, D.; Satzinger, K. J.; Smelyanskiy, V.; Strain, D.; Sung, K. J.; Szalay, M.; Takeshita, T. Y.; Vainsencher, A.; White, T.; Wiebe, N.; Yao, Z. J.; Yeh, P.; Zalcman, A. Hartree-Fock on a superconducting qubit quantum computer. *Science* **2020**, *369*, 1084–1089.
- (16) McClean, J. R.; Kimchi-Schwartz, M. E.; Carter, J.; De Jong, W. A. Hybrid quantum- classical hierarchy for mitigation of decoherence and determination of excited states. *Phys. Rev. A* **2017**, *95*, 042308.
- (17) Colless, J. I.; Ramasesh, V. V.; Dahlen, D.; Blok, M. S.; Kimchi-Schwartz, M. E.; McClean, J. R.; Carter, J.; de Jong, W. A.; Siddiqi, I. Computation of molecular spectra on a quantum processor with an error-resilient algorithm. *Phys. Rev. X* **2018**, *8*, 011021.
- (18) Higgott, O.; Wang, D.; Brierley, S. Variational quantum computation of excited states. *Quantum* **2019**, *3*, 156.
- (19) Nakanishi, K. M.; Mitarai, K.; Fujii, K. Subspace-search variational quantum eigen- solver for excited states. *Phys. Rev. Res.* **2019**, *1*, 033062.
- (20) Parrish, R. M.; Hohenstein, E. G.; McMahon, P. L.; Martínez, T. J. Quantum com-

- putation of electronic transitions using a variational quantum eigensolver. *Phys. Rev. Lett.* **2019**, *122*, 230401.
- (21) Ollitrault, P. J.; Kandala, A.; Chen, C.-F.; Barkoutsos, P. K.; Mezzacapo, A.; Pistola, M.; Sheldon, S.; Woerner, S.; Gambetta, J. M.; Tavernelli, I. Quantum equation of motion for computing molecular excitation energies on a noisy quantum processor. *Phys. Rev. Res.* **2020**, *2*, 043140.
- (22) Somma, R.; Ortiz, G.; Gubernatis, J. E.; Knill, E.; Laflamme, R. Simulating physical phenomena by quantum networks. *Phys. Rev. A* **2002**, *65*, 042323.
- (23) Chiesa, A.; Tacchino, F.; Grossi, M.; Santini, P.; Tavernelli, I.; Gerace, D.; Carretta, S. Quantum hardware simulating four-dimensional inelastic neutron scattering. *Nat. Phys.* **2019**, *15*, 455–459.
- (24) Francis, A.; Freericks, J.; Kemper, A. Quantum computation of magnon spectra. *Phys. Rev. B* **2020**, *101*, 014411.
- (25) Sun, S.-N.; Motta, M.; Tazhigulov, R. N.; Tan, A. T.; Chan, G. K.-L.; Minnich, A. J. Quantum computation of finite-temperature static and dynamical properties of spin systems using quantum imaginary time evolution. *PRX Quantum* **2021**, *2*, 010317.
- (26) Whitfield, J. D.; Biamonte, J.; Aspuru-Guzik, A. Simulation of electronic structure Hamiltonians using quantum computers. *Mol. Phys.* **2011**, *109*, 735–750.
- (27) Seeley, J. T.; Richard, M. J.; Love, P. J. The Bravyi-Kitaev transformation for quantum computation of electronic structure. *J. Chem. Phys.* **2012**, *137*, 224109.
- (28) Hastings, M. B.; Wecker, D.; Bauer, B.; Troyer, M. Improving quantum algorithms for quantum chemistry. *Quantum Inf. Comput.* **2015**, *15*, 1–21.
- (29) Motta, M.; Ye, E.; McClean, J. R.; Li, Z.; Minnich, A. J.; Babbush, R.; Chan, G. K.-L.

- Low rank representations for quantum simulation of electronic structure. *npj Quantum Inf.* **2021**, *7*, 1–7.
- (30) Song, C.; Xu, K.; Li, H.; Zhang, Y.-R.; Zhang, X.; Liu, W.; Guo, Q.; Wang, Z.; Ren, W.; Hao, J.; Feng, H.; Fan, H.; Zheng, D.; Wang, D.-W.; Wang, H.; Zhu, S.-Y. Generation of multicomponent atomic Schrödinger cat states of up to 20 qubits. *Science* **2019**, *365*, 574–577.
- (31) Nam, Y.; Chen, J.-S.; Pienti, N. C.; Wright, K.; Delaney, C.; Maslov, D.; Brown, K. R.; Allen, S.; Amini, J. M.; Apisdorf, J.; Beck, K. M.; Blinov, A.; Chaplin, V.; Chmielewski, M.; Collins, C.; Debnath, S.; Hudek, K. M.; Ducore, A. M.; Keesan, M.; Kreikemeier, S. M.; Mizrahi, J.; Solomon, P.; Williams, M.; Wong-Campos, J. D.; Moehring, D.; Monroe, C.; Kim, J. Ground-state energy estimation of the water molecule on a trapped-ion quantum computer. *npj Quantum Inf.* **2020**, *6*, 33.
- (32) Bravyi, S.; Kitaev, A. Y. Fermionic quantum computation. *Ann. Phys.* **2002**, *298*, 210–226.
- (33) Cai, X.; Fang, W.-H.; Fan, H.; Li, Z. Quantum computation of molecular response properties. *Phys. Rev. Res.* **2020**, *2*, 033324.
- (34) Tong, Y.; An, D.; Wiebe, N.; Lin, L. Fast inversion, preconditioned quantum linear system solvers, fast Green’s-function computation, and fast evaluation of matrix functions. *Phys. Rev. A* **2021**, *104*, 032422.
- (35) Chen, H.; Nusspickel, M.; Tilly, J.; Booth, G. H. Variational quantum eigensolver for dynamic correlation functions. *Phys. Rev. A* **2021**, *104*, 032405.
- (36) Harrow, A. W.; Hassidim, A.; Lloyd, S. Quantum algorithm for linear systems of equations. *Phys. Rev. Lett.* **2009**, *103*, 150502.

- (37) Ambainis, A. Variable time amplitude amplification and a faster quantum algorithm for solving systems of linear equations. *arXiv:1010.4458* **2010**,
- (38) Childs, A. M.; Kothari, R.; Somma, R. D. Quantum algorithm for systems of linear equations with exponentially improved dependence on precision. *SIAM J. Comput.* **2017**, *46*, 1920–1950.
- (39) Subaşı, Y.; Somma, R. D.; Orsucci, D. Quantum algorithms for systems of linear equations inspired by adiabatic quantum computing. *Phys. Rev. Lett.* **2019**, *122*, 060504.
- (40) Xu, X.; Sun, J.; Endo, S.; Li, Y.; Benjamin, S. C.; Yuan, X. Variational algorithms for linear algebra. *arXiv preprint arXiv:1909.03898* **2019**,
- (41) Bravo-Prieto, C.; LaRose, R.; Cerezo, M.; Subasi, Y.; Cincio, L.; Coles, P. J. Variational quantum linear solver. *arXiv preprint arXiv:1909.05820* **2019**,
- (42) McClean, J. R.; Romero, J.; Babbush, R.; Aspuru-Guzik, A. The theory of variational hybrid quantum-classical algorithms. *New J. Phys.* **2016**, *18*, 023023.
- (43) See Supplementary Materials for a comprehensive discussion of the VQR algorithm, device information, and details of experiments for each molecule.
- (44) Haung, K.; Wang, Z.-A.; Song, C.; Xu, K.; Li, H.; Wang, Z.; Guo, Q.; Song, Z.; Liu, Z.-B.; Zheng, D.; Deng, D.-L.; Wang, H.; Tian, J.-G.; Fan, H. Quantum generative adversarial networks with multiple superconducting qubits. *npj Quantum Inf.* **2021**, *5*, 1–5.
- (45) others,, et al. Metrological Characterization of Non-Gaussian Entangled States of Superconducting Qubits. *Phys. Rev. Lett.* **2022**, *128*, 150501.
- (46) Chuang, I. L.; Nielsen, M. A. Prescription for experimental determination of the dynamics of a quantum black box. *J. Mod. Opt.* **1997**, *44*, 2455.

- (47) Guo, Q.; Zheng, S.-B.; Wang, J.; Song, C.; Zhang, P.; Li, K.; Liu, W.; Deng, H.; Huang, K.; Zheng, D.; Zhu, X.; Wang, H.; Lu, C.-Y.; Pan, J.-W. Dephasing-insensitive quantum information storage and processing with superconducting qubits. *Phys. Rev. Lett.* **2018**, *121*, 130501.
- (48) Bonet-Monroig, X.; Sagastizabal, R.; Singh, M.; O'Brien, T. Low-cost error mitigation by symmetry verification. *Phys. Rev. A* **2018**, *98*, 062339.
- (49) Lanyon, B. P.; Whitfield, J. D.; Gillett, G. G.; Goggin, M. E.; Almeida, M. P.; Kaszal, I.; Biamonte, J. D.; Mohseni, M.; Powell, B. J.; Barbieri, M.; Aspuru-Guzik, A.; White, A. G. Towards quantum chemistry on a quantum computer. *Nat. Chem.* **2010**, *2*, 106–111.
- (50) Huber, K. P.; Herzberg, G. *Molecular Spectra and Molecular Structure IV. Constants of Diatomic Molecules*; Van Nostrand Reinhold, New York, 1979.
- (51) Clar, E.; Schoental, R. *Polycyclic hydrocarbons*; Springer, 1964; Vol. 1.
- (52) Anthony, J. E. Functionalized acenes and heteroacenes for organic electronics. *Chem. Rev.* **2006**, *106*, 5028–5048.
- (53) Szalay, P. G.; Muller, T.; Gidofalvi, G.; Lischka, H.; Shepard, R. Multiconfiguration self-consistent field and multireference configuration interaction methods and applications. *Chem. Rev.* **2012**, *112*, 108–181.
- (54) Ma, Y.; Chen, C.; Meigs, G.; Randall, K.; Sette, F. High-resolution K-shell photoabsorption measurements of simple molecules. *Phys. Rev. A* **1991**, *44*, 1848.
- (55) Püttner, R.; Dominguez, I.; Morgan, T.; Cisneros, C.; Fink, R.; Rotenberg, E.; Warwick, T.; Domke, M.; Kaindl, G.; Schlachter, A. Vibrationally resolved O 1s core-excitation spectra of CO and NO. *Phys. Rev. A* **1999**, *59*, 3415.

- (56) Norman, P.; Dreuw, A. Simulating x-ray spectroscopies and calculating core-excited states of molecules. *Chem. Rev.* **2018**, *118*, 7208–7248.
- (57) Besley, N. A. Modeling of the spectroscopy of core electrons with density functional theory. *Wiley Interdiscip. Rev. Comput. Mol. Sci.* **2021**, e1527.
- (58) Endo, S.; Cai, Z.; Benjamin, S. C.; Yuan, X. Hybrid quantum-classical algorithms and quantum error mitigation. *J. Phys. Soc. Japan* **2021**, *90*, 032001.